THE JOURNAL OF BIOLOGICAL CHEMISTRY VOL. 288, NO. 32, pp. 23529–23542, August 9, 2013

A Reaction Center-dependent Photoprotection Mechanism in a Highly Robust Photosystem II from an Extremophilic Red Alga, *Cyanidioschyzon merolae*[*] [S]

Received for publication, May 13, 2013, and in revised form, June 7, 2013 Published, JBC Papers in Press, June 17, 2013, DOI 10.1074/jbc.M113.484659

Tomasz Krupnik[‡], Eva Kotabová[§¶1], Laura S. van Bezouwen[‖], Radosław Mazur[**], Maciej Garstka[**], Peter J. Nixon[‡‡], James Barber[‡‡], Radek Kaňa[§¶1], Egbert J. Boekema[‖], and Joanna Kargul[‡2]

From the [‡]Department of Plant Molecular Physiology, Faculty of Biology, University of Warsaw, Miecznikowa 1, 02-096 Warsaw, Poland, the [§]Laboratory of Photosynthesis, Institute of Microbiology, Academy of Sciences, Opatovicky Mlyn, CZ-379 81 Třeboň, Czech Republic, the [¶]Faculty of Sciences, University of South Bohemia, Branišovská 31, 370 05 České Budějovice, Czech Republic, the [‖]Electron Microscopy Group, Groningen Biomolecular Sciences and Biotechnology Institute, University of Groningen, Linnaeusborg, Nijenborgh 7, 9747 AG Groningen, The Netherlands, the [**]Department of Metabolic Regulation, Faculty of Biology, University of Warsaw, Miecznikowa 1, 02-096 Warsaw, Poland, and the [‡‡]Department of Life Sciences, Imperial College London, S. Kensington Campus, London SW7 2AZ, United Kingdom

Background: PSII is a protein complex that captures sunlight to drive water oxidation.
Results: *Cyanidioschyzon merolae* PSII is protected by reversible reaction center-based non-photochemical quenching.
Conclusion: *C. merolae* PSII employs reaction center non-photochemical quenching as the main photoprotective mechanism.
Significance: We provide the first direct evidence of the PSII reaction center as the primary locus of non-photochemical quenching in the extremophilic red algae.

Members of the rhodophytan order *Cyanidiales* are unique among phototrophs in their ability to live in extremely low pH levels and moderately high temperatures. The photosynthetic apparatus of the red alga *Cyanidioschyzon merolae* represents an intermediate type between cyanobacteria and higher plants, suggesting that this alga may provide the evolutionary link between prokaryotic and eukaryotic phototrophs. Although we now have a detailed structural model of photosystem II (PSII) from cyanobacteria at an atomic resolution, no corresponding structure of the eukaryotic PSII complex has been published to date. Here we report the isolation and characterization of a highly active and robust dimeric PSII complex from *C. merolae*. We show that this complex is highly stable across a range of extreme light, temperature, and pH conditions. By measuring fluorescence quenching properties of the isolated *C. merolae* PSII complex, we provide the first direct evidence of pH-dependent non-photochemical quenching in the red algal PSII reaction center. This type of quenching, together with high zeaxanthin content, appears to underlie photoprotection mechanisms that are efficiently employed by this robust natural water-splitting complex under excess irradiance. In order to provide structural details of this eukaryotic form of PSII, we have employed electron microscopy and single particle analyses to obtain a 17 Å map of the *C. merolae* PSII dimer in which we locate the position of the protein mass corresponding to the additional extrinsic protein stabilizing the oxygen-evolving complex, PsbQ′. We conclude that this lumenal subunit is present in the vicinity of the CP43 protein, close to the membrane plane.

Photosystem II (PSII)[3] is a multimeric transmembrane complex present in the thylakoid membranes of cyanobacteria, algae, and higher plants that is able to capture solar energy and use it to drive charge separation and water oxidation catalysis. Recently, the crystal structure of PSII isolated from the thermophilic cyanobacterium *Thermosynechococcus vulcanus* has been reported at a resolution of 1.9 Å (1). This atomic structure has facilitated formation of the working models for understanding the water-splitting reaction based on the previous crystallographic structures of cyanobacterial PSII (2–9). The cyanobacterial complex contains 20 protein subunits with a total molecular mass of 350 kDa. Bound within these subunits are over 1,300 water molecules and 85 cofactors: 35 chlorophyll (Chl) molecules, two pheophytins, 11 β-carotenes, over 20 lipids, two plastoquinones, two heme irons, one non-heme iron, four manganese atoms, 3–4 Ca^{2+} ions, three Cl^{-} ions, and one bicarbonate (1). The catalytic site is composed of a Mn_4Ca cluster surrounded by a number of highly conserved amino acids, mainly derived from the D1 reaction center (RC) subunit and

* This work was supported in part by the Polish Ministry of Science and Higher Education and by European Science Foundation Grant 844/N-ESFEuroSolarFuels/10/2011/0 (to J. K.) and was partially performed with the use of CePT infrastructure financed by the European Union (European Regional Development Fund within the Operational Program "Innovative Economy" for 2007–2013) (to R. M. and M. G.).
[S] This article contains supplemental Table S1 and an additional reference.
[1] Supported by Czech Republic Academy of Sciences Project GACR P501-12-0304 and Project Algatech (CZ.1.05/2.1.00/03.0110).
[2] To whom correspondence should be addressed. Tel.: 48-225-542-005; Fax: 48-225-543-910; E-mail: j.kargul@biol.uw.edu.pl.

[3] The abbreviations used are: PSII, photosystem II; PSI, photosystem I; AEC, anion exchange chromatography; Chl, chlorophyll; DCMU, 3-(3,4-dichlorophenyl)-1,1-dimethylurea; DDM, dodecyl-β-D-maltoside; F_0, minimal fluorescence; F_V, variable fluorescence; F_M, maximal fluorescence of dark-adapted samples; F_M', maximal fluorescence in light; F_V/F_M, maximal quantum yield of PSII; NPQ, non-photochemical quenching; OEC, oxygen evolving complex; RC, reaction center; SEC, size exclusion chromatography; σ_{PSII}, effective antennae size of PSII; Zea, zeaxanthin; μE, microeinstein(s); Tricine, *N*-[2-hydroxy-1,1-bis(hydroxymethyl)ethyl]glycine; qE, high energy quenching; qZ, slowly inducible quenching.

one from the CP43 inner antenna subunit. The model that places three manganese ions and a calcium ion at the corner of a cubane with oxo-bridges and the fourth manganese linked to the cubane via a bridging oxygen (2) has gained support in the latest atomic structure of PSII (1) as well as from quantum mechanical and x-ray spectroscopic considerations (10–13).

Although we now have a detailed structural model of PSII from cyanobacteria at an atomic resolution, no corresponding structure of the eukaryotic PSII complex has been published to date. Hence, there is an urgent need to purify a highly stable eukaryotic PSII complex that would prove suitable for high resolution structural analysis. Equally important, PSII as nature's water-splitting enzyme provides a blueprint in terms of the catalytic rate of water oxidation in ambient conditions for the construction of stable synthetic catalysts operating within solar-to-fuel nanodevices (14–17). A logical approach toward these goals is to obtain a eukaryotic form of PSII using an organism that is likely to provide a robust and highly active form of the complex. To this end, we isolated and characterized the dimeric PSII complex from the extremophilic unicellular red alga *Cyanidioschyzon merolae*.

C. merolae belongs to the rhodophytan order *Cyanidiales*, whose members thrive in acidic hot springs (18) and are unique among phototrophs in the ability to live at extremely low pH (pH 0.2–4) and moderately high temperatures (40–56 °C). Despite such an extremely acidic environment, the intracellular pH of these algae is most likely neutral due to the active H^+ efflux across the plasma membrane (19). *C. merolae* is considered to be one of the most primitive eukaryotic phototrophs because it diverged near the root of the red algal lineage that forms a basal group within the photosynthetic eukaryotes (20). The photosynthetic apparatus of this alga is regarded as the closest equivalent of the prokaryotic ancestor of the present day chloroplast (21). As an evolutionary intermediate between the photosynthetic apparatus of prokaryotic cyanobacteria and that of the eukaryotes in the green lineage, it contains a mixture of prokaryotic and eukaryotic structural traits. Whereas red algal photosystem I (PSI) resembles a higher plant complex, with an crescent-shaped Chl*a*-binding light-harvesting antenna system asymmetrically bound on one side of the core complex (22–23), PSII of red algae is structurally similar to the cyanobacterial counterpart in that it contains light-harvesting antenna composed of phycobilisomes, large peripheral membrane complexes formed by phycobiliproteins, instead of Chl*a*/*b*-binding antenna proteins that constitute the light-harvesting system of green algae and higher plants.

The oxygen-evolving complex (OEC) in *C. merolae* PSII is stabilized by four extrinsic lumenal subunits: cyanobacteria-like PsbV and PsbU, the evolutionarily conserved PsbO subunit, and an additional 20-kDa subunit PsbQ′ distantly related to the higher plant and green algal PsbQ polypeptides (24). The precise localization of this subunit and its role in stabilization of the OEC are currently unknown, although low resolution single particle analysis and *in vitro* reconstitution experiments suggested that the red algal PsbQ′ may independently associate with the PSII core complex in the close vicinity of PsbV and the PsbU subunits and is required for effective binding of these extrinsic subunits (22, 25). In contrast, PsbQ in higher plants functionally associates with PSII via its direct interaction with both PsbO and PsbP extrinsic subunits, stabilizing the OEC (reviewed in Ref. 26). Interestingly, PsbQ′ can functionally replace PsbQ in spinach during cross-reconstitution experiments despite the low amino acid sequence homology between both proteins (25). The binding mode for another OEC subunit, PsbV, also differs between cyanobacteria and red alga. In red algae, PsbV binds via other extrinsic subunits, whereas its cyanobacterial counterpart binds directly with the PSII core (reviewed in Ref. 26). All of these lines of evidence point toward significant structural differences on the lumenal side of the PSII complex that was formed at various evolutionary stages.

It is well established that under conditions of excessive irradiation (*i.e.* when light energy absorption exceeds the capacity and demands of photosynthesis), several photoprotective and optimizing mechanisms are triggered. These mechanisms include regulation of light absorption capacity between PSI and PSII (state transitions; see Ref. 27), fast D1 protein turnover during photoinhibition of PSII, and photoprotective non-photochemical quenching (see Refs. 28 and 29 for recent reviews). Non-photochemical quenching (NPQ) represents a feedback regulatory mechanism that leads to dissipation of excessive light either in the light-harvesting antennae (29) or in the reaction center of PSII (30). The most flexible and dominant component of NPQ, ΔpH-dependent high energy quenching (qE) is a major photoprotective strategy that operates on a time scale of seconds to minutes.

Although mechanistic aspects and molecular components of pH-dependent qE have been widely studied in higher plants and green algae, little is known about molecular mechanisms of PSII fluorescence quenching in phycobilisome-containing red algae. In the red algae ancestor, prokaryotic cyanobacteria, excessive light is dissipated in phycobilisomes, aided by the orange carotenoid protein that is absent in red algae (31). The detailed NPQ mechanisms in red algae are largely unknown, and the NPQ properties are mostly derived from *in vivo* fluorescence measurements in intact cells. Kirilovsky and colleagues (32, 33) demonstrated the existence of ΔpH-dependent quenching in *Rhodella violacea* and *Porphyridium cruentum* strains of mesophylic red algae. These authors have suggested that, in contrast to higher plants and green algae, the dominant part of NPQ in red algae might occur in the RC rather than in the antenna (33). Several photochemical mechanisms have been suggested for the RC type of quenching (reviewed in Ref. 34). Although the real importance and extent of RC quenching in photoprotection is still a matter of debate, especially in comparison with qE in antennae (compare Refs. 29 and 30), the existence of this type of quenching has been proved for PSII isolated from various photothrophs (35, 36). However, the same direct evidence has been missing for red algae.

Here we report a detailed structural and functional analysis of a highly active and robust dimeric PSII complex isolated from *C. merolae*. We provide the first direct evidence that the red algal PSII complex is rich in zeaxanthin and employs reversible RC-based non-photochemical quenching that is triggered by low pH. These features provide the basis for the remarkable robustness of this complex across a range of extreme light, temperature, and pH conditions. In the first attempt to provide

structural details of this eukaryotic form of PSII, we have employed electron microscopy (EM) and single particle analyses to produce a two-dimensional electron density map in which we locate the position of the additional protein mass over and above that found in cyanobacterial PSII. We attribute this mass to the PsbQ′ subunit, which binds to the OEC in the vicinity of the CP43 protein, close to the membrane plane.

MATERIALS AND METHODS

Cell Culturing and Isolation of Thylakoids—*C. merolae* strain NIES-1332 was obtained from the Microbial Culture Collection of the National Institute for Environmental Studies (Tsukuba, Japan). Liquid cultures of the *C. merolae* cells were grown in a Versatile Environmental Test Chamber (Sanyo, Japan) in standard 250-ml tissue flasks oriented in an upright position. Cells were suspended in 50 ml of Allen 2 medium, pH 2.5 (37), at 42 °C under continuous 90-μE white light illumination with shaking at 115 rpm. Small scale cultures were grown to OD_{680} ~2.5 and then subcultured into 1-liter interim cultures and finally grown as 10-liter cultures in Allen 2 medium until late log phase (until OD_{682} 3.5) in the presence of 5% CO_2 administered at a constant flow rate of 3 liters/min under 150-μE continuous white light illumination. For thylakoid preparation, cells were harvested at OD_{680} ~2.5 by centrifugation at 5,000 rpm at 4 °C for 10 min. Cell pellets were washed with 50–100 ml of low ionic strength buffer A (40 mM MES-KOH, pH 6.1, 10 mM $CaCl_2$, 5 mM $MgCl_2$, 25% (w/v) glycerol) and then resuspended in 50 ml of buffer A supplemented with 50 μg/ml DNase I and the Complete™ protease inhibitor mixture (Roche Applied Science). Cells were ruptured by vigorous agitation with 0.1-mm glass beads in a BeadBeater (BioSpec) using 13 cycles of 10 s and interim 4-min cooling off periods. Cell lysate was separated from beads by vacuum filtration. Thylakoids were pelleted by centrifugation at 104,200 × *g* for 30 min at 4 °C and washed once with buffer A. Final thylakoid pellets were resuspended in buffer A at a Chl concentration of 2–2.5 mg/ml, snap-frozen in liquid N_2, and stored at −70 °C prior to use.

Purification of PSII—Purification of the dimeric PSII complex was performed according to a modified protocol of Adachi *et al.* (38). Thylakoids (1 mg/ml Chl) were solubilized with 1% (w/v) dodecyl-β-D-maltoside (DDM; Biomol) at 4 °C for 40 min in the dark. Solubilized membranes were centrifuged at 104,200 × *g* for 30 min at 4 °C, and the filtered supernatants were applied onto a DEAE TOYOPEARL 650 M column equilibrated with buffer A (40 mM MES-KOH, pH 6.1, 10 mM $CaCl_2$, 5 mM $MgCl_2$, 25% (w/v) glycerol) supplemented with 0.03% DDM. The loaded column was washed with 2 column volumes of the medium ionic strength buffer (0.09 M NaCl, 40 mM MES-KOH, pH 6.1, 3 mM $CaCl_2$, 25% (w/v) glycerol, 0.03% (w/v) DDM), and crude PSII was eluted with the high ionic strength buffer (0.23 M NaCl, 40 mM MES-KOH, pH 6.1, 3 mM $CaCl_2$, 25% (w/v) glycerol, 0.03% (w/v) DDM). The PSII-containing fractions were pooled and dialyzed overnight in 5 liters of buffer A containing 0.03% DDM at 4 °C in the dark. Crude PSII was loaded onto a DEAE TOYOPEARL 650 S column equilibrated with buffer A supplemented with 0.03% DDM. After washing the column with 3 column volumes of the wash buffer (0.05 M NaCl, 40 mM MES-KOH, pH 6.1, 3 mM $CaCl_2$, 25% (w/v) glycerol, 0.03% DDM), pure PSII (devoid of residual free carotenoids and phycobilisomes) was eluted with a continuous NaCl gradient (0.05–0.15 M NaCl, 40 mM MES-KOH, pH 6.1, 3 mM $CaCl_2$, 25% (w/v) glycerol, 0.03% DDM) to separate PSII monomers and dimers. Fractions containing PSII dimers were identified by size exclusion chromatography (SEC), using a Biosep SEC-4000 column (Phenomenex, Torrance, CA) equilibrated with a carrier buffer (20 mM MES-KOH, pH 6.5, 10 mM $MgCl_2$, 3 mM $CaCl_2$, 0.5 M mannitol, 0.05% DDM) at 2 ml/min. PSII dimer fractions were pooled and then concentrated using VivaSpin-20 (100,000 molecular weight cut-off) concentrators (Sartorius Stedim) to at least 2 mg/ml Chl and stored upon snap freezing at −70 °C until further use.

PSII Activity Measurement—Functional activity of the isolated PSII (5 μg of Chl) was measured using an oxygen Clark-type electrode (Hansatech). Measurements were performed at 30 °C in buffer A in the presence of 0.125 mM 2,6-dichloro-*p*-benzoquinone (Sigma) and 2.5 mM potassium ferricyanide (POCH, Gliwice, Poland) as the exogenous electron acceptors. Samples (1 μg/ml Chl) were illuminated with a standard white light intensity of 6,000 $\mu E/m^2/s$ or as described, using a KL 2500 LCD white light source (Schott, Mayence, Germany). Activities were calculated from initial rates of oxygen evolution curves. The values of light intensity (600–25,000 $\mu E/m^2/s$), temperature (15–55 °C), and buffer pH (3–7.5) were permutated, depending on the experimental settings. The herbicide sensitivity of the Q_B site was monitored following preincubation of PSII for 1 min in the dark with 0.001–20 μM 3-(3,4-dichlorophenyl)-1,1-dimethylurea (DCMU; Sigma) prior to oxygen evolution measurement under standard conditions. Each measurement was repeated three times for each DCMU concentration.

Carotenoid Content Analysis—Analytical HPLC was performed according to a modified method described before (39), using a maximum flow rate of 1 ml/min and a Nucleosil 100 C18 column (Teknokroma, Barcelona, Spain). Pigments were extracted from cells grown at 90 $\mu E/m^2/s$ and the corresponding PSII samples (0.5 mg Chl) with a 1-ml acetone/methanol (7:2, v/v) mixture. The extract was concentrated to 1 mg/ml Chl, and samples (20 μg of Chl) were analyzed on a C18 column. The content of each carotenoid species was expressed as a ratio of the area under the pigment-corresponding peak to the area under the Chl peak. Pigment molar ratios were calculated using extinction coefficients of 83.2, 91.7, and 125.3 $mM^{-1}\ cm^{-1}$ for zeaxanthin, Chl*a*, and β-carotene, respectively (40).

LC-MS/MS Identification of PSII Proteins—PSII proteins after acetone precipitation were dissolved in 0.1% (w/v) RapiGest™ surfactant (Waters) in 50 mM ammonium bicarbonate. After reduction and subsequent alkylation of cysteine residues, proteins were digested in sequencing grade trypsin (Sigma-Aldrich) at 30 °C overnight. Reaction was stopped by the addition of trifluoroacetic acid to 1% (v/v) final concentration. For small PSII subunits that do not contain trypsin cleavage sites, additional digestion in solution as well as in-gel digestions with chymotrypsin (Sigma-Aldrich) were carried out. Digested peptides were separated using a NanoAcquity Ultra Performance LC system (Waters) connected with a mass spectrometer. Peptides were loaded onto a Symmetry® C18 (5 μm;

180 μm × 20 mm) trap column (Waters) at a flow rate of 10 μl/min in 99% buffer A (0.1% formic acid in water) and 1% buffer B (0.1% formic acid in acetonitrile) for 3 min. Trapped peptides were separated on a BEH 130 C18 (1.7 μm; 75 μm × 200 mm) analytical column (Waters) equilibrated in 97% buffer A and 3% buffer B. The column was eluted at a constant flow rate of 300 nl/min at 35 °C with a linear gradient of buffer B distributed as follows: 3–40% B in the first 145 min; 40–85% B in 145–151 min; and 85% B in 151–165 min. In the next 5 min, concentration of buffer B was decreased from 85 to 3%, and the column was equilibrated for an additional 10 min before the next injection. Online MS^E analyses were performed in a positive ionization mode on the Synapt G2 HDMS mass spectrometer (Waters). Fragmentation spectra were recorded in the range of 50–2,000 Da (1.0 s/single scan), and the transfer collision energy was ramped in the range of 15–35 V. The mass accuracy of the raw data was corrected using leucine enkephalin (2 ng/μl, 1 μl/min flow rate, 556.2771 Da/e $[M + H]^+$) that was infused into the mass spectrometer as a lock mass during sample analysis. Each sample was analyzed at least three times and was mixed with bovine serum albumin tryptic digest (60 fmol) as an internal standard. For protein identification, peak lists were created from the raw data sets and used to search for proteins in a randomized *C. merolae* protein data bank using ProteinLynx Global Server version 2.4 software (Waters).

77 K Fluorescence Measurement—Steady-state fluorescence spectra were collected using a modified Shimadzu RF-5301PC spectrofluorometer (41) at 77 K and excitation wavelengths of 440 and 580 nm. PSII samples (10 μg/ml Chl) in a buffer composed of 40 mM MES, pH 6.1, 10 mM $CaCl_2$, 5 mM $MgCl_2$, 25% (w/v) glycerol, and 0.03% (w/v) DDM were loaded into prechilled cuvettes and then frozen in liquid nitrogen for 5 min in the dark prior to collecting emission spectra.

Room Temperature Absorbance and Redox Spectroscopy—All measurements were carried out at room temperature using a Shimadzu UV 1800 spectrophotometer. To estimate the content of cytochrome c_{550} and cytochrome b_{559}, redox difference spectra (oxidized − reduced) were calculated. For redox spectroscopy, the PSII dimer was diluted to 0.01 mg/ml Chl. 1 ml of the sample was used to prepare the base line in the wavelength range between 600 and 500 nm. Subsequently, a grain of potassium ferricyanide ($K_3[Fe(CN)_6]$; POCH) was mixed with the sample for 30 s to oxidize the total cytochrome pool prior to collection of the oxidized spectra. For the reduction of cytochromes, a 1-ml sample from the same PSII suspension was mixed with a grain of sodium dithionite ($Na_2S_2O_4$; POCH) for 30 s. prior to collection of the reduced absorbance spectra. To ensure complete oxidation or reduction of cytochromes, an additional grain of ferricyanide or dithionite was added before reacquiring the oxidized and reduced spectra, respectively. The cytochrome c_{550} concentration was calculated from the maximal absorption at 550 nm and the extinction coefficient of 27.0 mM^{-1} cm^{-1} (42). For calculation of the cytochrome b_{559} content, maximum absorbance at 557 nm and an extinction coefficient of 25.1 mM^{-1} cm^{-1} were used (42). Each spectrum was recorded three times.

In Vivo Chlorophyll a Fluorescence and Non-photochemical Quenching—An FL-100 fluorometer (Photon Systems Instruments, Brno, Czech Republic) has been used for measurements of NPQ of maximal fluorescence *in vivo*. Fluorescence signal was detected in the 690–750 nm range. Maximal fluorescence of dark-adapted cells (F_M) was measured at a saturating flash (466 nm; Δt = 500 ms; ~2,000 $\mu E/m^2/s$) applied before and after a short period of low intensity blue light (466 nm; duration 60 s; intensity 7 $\mu E/m^2/s$). The same setup has been used to exclude the effect of state transitions on the F_M value during phycobilisome binding in cyanobacteria (31). NPQ was induced by blue actinic light (466 nm; $\Delta\lambda$, 20 nm; 750 $\mu E/m^2/s$, duration 150 s). NPQ value was calculated from quenching of maximal fluorescence in light (F_M') at a saturation flash (466 nm; Δt = 500 ms; ~2,000 $\mu E/m^2/s$), according to the Stern-Volmer formula, $NPQ = (F_M - F_M')/F_M'$. Recovery from the NPQ state was measured in the dark following a given light period. Cells used for *in vivo* measurements were cultivated in the thermostated bioreactor (38 °C) bubbled with air, at a continuous irradiation of 80 $\mu E/m^2/s$.

Variable Fluorescence and Effective Antenna Size Measurement in Vitro—Variable fluorescence (F_V) and the effective antennae size of pure PSII (σ_{PSII}) were measured with a custom designed fluorometer FL3500 (Photon Systems Instruments) equipped with a fast repetition rate fluorescence protocol. The single-turnover flash was induced by application of a series of short subsaturating flashes (1.5 μs long, λ = 463 nm) to dark-adapted samples (*e.g.* see Ref. 43). The measured fluorescence rise during the single turnover flash was fitted according to the model described before (44), giving the effective PSII cross-section parameter σ_{PSII} (43). Variable fluorescence (F_V) was calculated as a difference between maximum (F_M) and minimal (F_0) fluorescence measured before (F_0) and after (F_M) application of saturating flashes. For measurements at various pH values, purified dimeric PSII samples (0.15–0.2 μg Chl/ml) were resuspended in the thermostated (22 °C) buffer containing 40 mM MES, 10 mM $CaCl_2$, 5 mM $MgCl_2$, 25% (w/v) glycerol, and 0.03% (w/v) DDM, in a pH range of 3–7.5. Samples were kept in the dark for 2 min in a buffer of given pH prior to the fluorescence measurement. The reversibility of pH-induced changes was tested by incubating the concentrated sample for 2 min in a buffer of particular pH, followed by transfer to pH 7 by the addition of an appropriate amount of KOH. After a 4-min recovery at pH 7, the sample was used for fluorescence measurements. In all measurements, 1,4-benzoquinone (22.6 μM) and potassium ferricyanide (48.8 μM) were used as the exogenous electron acceptors of PSII.

SDS-Polyacrylamide Gel Electrophoresis—SDS-PAGE was carried out using the Tris-Tricine system (45, 46). Protein bands (5 μg of Chl/lane) were resolved overnight on an 18% polyacrylamide gel in the presence of 6 M urea at a constant voltage of 25 V. Proteins were visualized with Coomassie Brilliant Blue R-250 using standard procedures. Prior to SDS-PAGE, samples were treated with 4 volumes of ether/methanol (1:1, v/v) overnight at −20 °C to remove pigments. Total protein was collected by centrifugation at 13,500 rpm at 4 °C for 10 min, air-dried at room temperature, and then resuspended in 200 μl of 1× SDS-PAGE sample buffer (12% (w/v) SDS, 30%

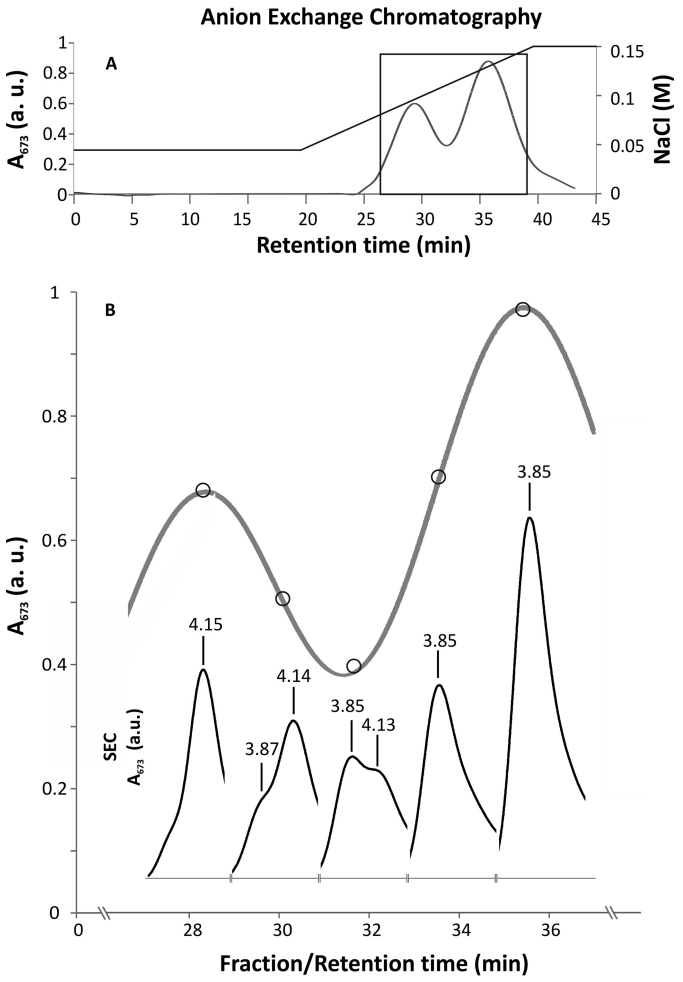

FIGURE 1. **Anion exchange chromatography purification of the *C. merolae* PSII dimer.** *A*, AEC chromatogram from the second step of PSII purification on a DEAE ToyoPearl 650 S column. *B*, selected section of the AEC chromatogram (*boxed* in *A*). Elution fractions were analyzed by SEC (*inset*). The SEC chromatogram of every fraction analyzed is positioned directly below a circle that marks the position of the corresponding fraction in the AEC chromatogram. Consecutive SEC chromatograms show a transition between the PSII monomer and dimer (retention times of 4.15 and 3.85 min, respectively). *a.u.*, arbitrary units.

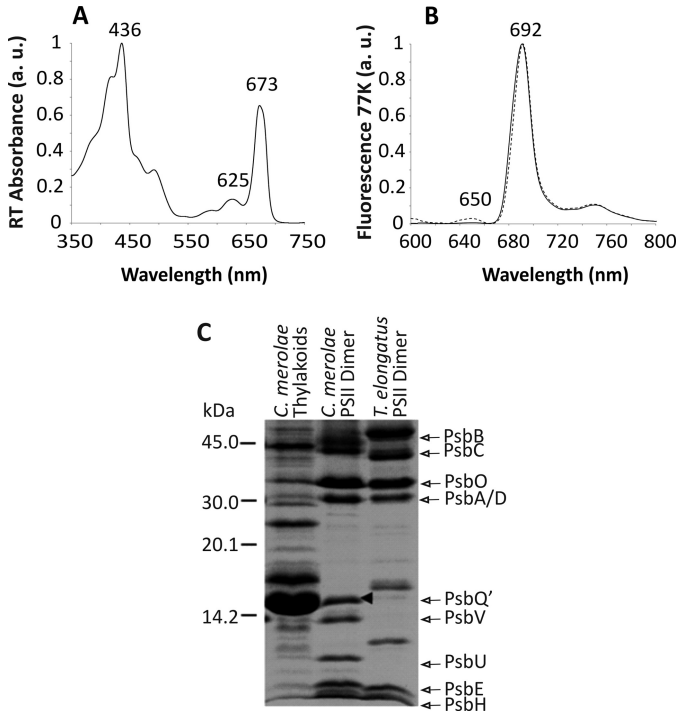

FIGURE 2. **Spectroscopic and compositional analyses of the *C. merolae* PSII dimer.** Room temperature absorbance spectrum of PSII dimer (*A*) shows the red peak at 673 nm, characteristic of PSII. The PSII complex purity was expressed as a ratio of A_{673}/A_{625} and was estimated at ~5, confirming a complete removal of residual phycobilisomes. The 77 K steady-state fluorescence emission spectra (*B*) were taken at excitation wavelengths of 440 nm (*solid line*) and 580 nm (*dashed line*). The excitation wavelength of 580 nm was used to detect any residual contamination with phycobilisomes that emit fluorescence at 625 nm. The 440-nm wavelength excited Chl*a* to produce a symmetric emission peak at 692 nm, characteristic of PSII. *C*, SDS-PAGE protein profile of the *C. merolae* PSII dimer. Samples (5 μg of Chl/lane) were resolved on a 18% Tris-Tricine gel. The positions of PsbA/C and PsbB/C as well as PsbO, PsbQ′, PsbV, and PsbU were identified by Western blotting and MS/MS analyses. The position of PsbQ′ is marked with an *arrowhead* in *C*. *a.u.*, arbitrary units.

(w/v) glycerol, 0.05% (w/v) Coomassie Blue G-250, 150 mM Tris-HCl, pH 7.0).

Electron Microscopy—Protein samples were negatively stained with 2% uranyl acetate on glow-discharged carbon-coated copper grids. Images were recorded on a Philips CM120 electron microscope with a LaB_6 filament, operating at 120 kV, with a Gatan 4000 SP 4K slow scan CCD camera. The magnification used was ×133,000, compatible with a pixel size (after binning the images) of 2.25 Å at the specimen level. GRACE software was used for semiautomated data acquisition (47). From about 2,000 recorded EM images, over 20,000 particle projections were selected. Processing of single particles was performed with the Groningen image-processing (Grip) software package, including multireference alignments, multivariate statistical analysis, and classification. The resolution of the final EM maps was determined with Fourier ring correlation and the 3σ criterion (48) and was calculated at 17 Å.

RESULTS

Purification and Compositional Analysis of the C. merolae PSII Dimer—We set out to purify a highly active, intact, and homogenous preparation of the *C. merolae* dimeric PSII with the aim of examining its capacity to adapt to various extreme conditions as well as obtaining the insight into the eukaryotic PSII molecular structure. Following solubilization of thylakoids with DDM, we separated PSII monomers and dimers using a two-step anion exchange chromatography (AEC) approach (see Fig. 1*A*). In the second step, we purified a robust and highly active PSII dimer (yield 3.5%) that was stable for up to 120 h of dark incubation at 17 °C (see Fig. 3*B*). The homogeneity of the sample was verified by SEC, which showed a single elution peak with a retention time corresponding to the PSII dimer (Fig. 1*B*). The purity of the PSII complex was additionally confirmed spectroscopically by identification of characteristic peaks at 673 nm in the room temperature absorbance spectrum and 692 nm in the 77 K emission spectrum (see Fig. 2, *A* and *B*), similar to other red algal PSII preparations from *Cyanidium caldarium* and *P. cruentum* (22, 49). The PSII dimer purity was monitored for each AEC fraction by measuring a ratio of A_{673}/A_{625}. For the pure dimeric PSII preparation free of phycobilisomes, the A_{673}/A_{625} ratio was estimated at ~5, yielding 99% homogeneous sample.

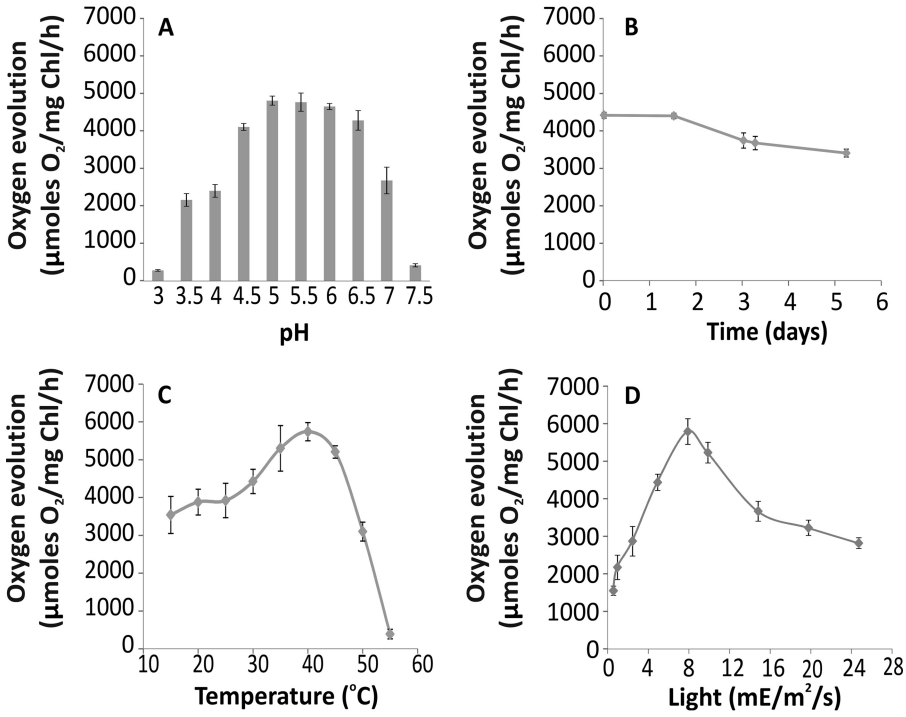

FIGURE 3. **PSII activity is sustained in various extreme conditions.** *A*, PSII maintains nearly full activity of 4,500 μmol of O_2/mg of Chl/h in a relatively broad range of pH (between 5 and 6.5) with standard 5,000 μE/m^2/s light intensity and 30 °C. *B*, when stored at 17 °C for a period of 5 days, PSII retains nearly 80% of its activity measured in standard conditions. *C*, PSII has a distinctive temperature optimum, with a maximum activity at 40 °C, measured in standard conditions. *D*, upon increasing light intensity, PSII reaches a maximum activity of ~6,000 μmol O_2/mg Chl/h at 8,000 μE/m^2/s, which lowers to 3,000 μmol of O_2/mg of Chl/h at 25,000 μE/m^2/s. Each data point represents an average value from three independent measurements. *Error bars*, S.D.

We then analyzed the subunit composition of the purified *C. merolae* PSII dimer by biochemical and mass spectrometry approaches. Fig. 2*C* and supplemental Table S1 show that the reaction center subunits (D1 and D2), inner antenna subunits (CP43 and CP47), four extrinsic subunits stabilizing the OEC (PsbO, PsbU, PsbV, and PsbQ′), and the majority of small intrinsic subunits were all present in our preparation. In addition, we detected an auxiliary subunit Psb27 and low molecular weight subunit PsbW in our dimer preparations (see supplemental Table S1).

We estimated the stoichiometry of PSII/cytochrome c_{550} (PsbV) and PSII/cytochrome b_{559} by measuring redox difference spectra in the presence of ferricyanide (oxidized) or dithionite (reduced). The redox difference spectra showed two characteristic peaks at 550 and 557 nm, corresponding to the fully reduced forms of cytochrome c_{550} and cytochrome b_{559}, respectively (data not shown). The molar ratios of PSII/cytochrome c_{550} and PSII/cytochrome b_{559} were estimated at 0.954 ± 0.014 and 0.953 ± 0.038, respectively, indicating 1:1 stoichiometry of both cytochromes and PSII (data not shown).

Biochemical Activity and Robustness of the C. merolae PSII—First, we tested the herbicide sensitivity of the Q_B site to DCMU. We observed rapid inactivation of oxygen-evolving activity upon the DCMU treatment, with inhibition of more than 95% of PSII activity at a 10 μM concentration of the herbicide (data not shown). We estimated the value of the inhibition constant K_i at 0.46 ± 0.012 μM DCMU, using the Dixon analysis (50). This value agrees well with the previously reported K_i value of 0.33 μM for DCMU inhibition in spinach thylakoids (51) or in isolated *Thermosynechococcus elongatus* PSII (52).

We then proceeded with a detailed examination of the catalytical activity of the *C. merolae* PSII complex across a broad range of extreme conditions (see Fig. 3). The oxygen-evolving activity of PSII varied between 4,000 and 6,000 μmol of O_2/mg of Chl/h for different preparations, with an average activity of 4,500 μmol of O_2/mg of Chl/h under the standard experimental conditions (30 °C, pH 6.3, white light of 5,000 – 8,000 μE/m^2/s). It was one of the highest recorded oxygen-evolving activities obtained under our standard experimental conditions and exceeded that of PSII isolated from the thermophilic cyanobacteria used to obtain the x-ray structures of the complex (1–3, 53). Moreover, the *C. merolae* dimeric PSII complex maintained its full activity in a relatively broad range of pH (between 5 and 6.5) when illuminated with white light of 5,000 μE/m^2/s at 30 °C (see Fig. 3*A*). It also exhibited a distinctive temperature optimum, with a maximum activity at 40 °C, when measured in standard conditions (see Fig. 3*C*). Moreover, the *C. merolae* PSII dimer retained its average oxygen-evolving activity when illuminated with high white light intensities (up to 20,000 μE/m^2/s; see Fig. 3*D*), indicating that the oxygen-evolving complex remained intact when subjected to light intensities well in excess of the saturation level.

We determined the total pigment composition of *C. merolae* cells and of PSII dimers, using HPLC analysis (see Fig. 4 and Table 1). Both carotenoids and Chl*a* were detected at 437 nm, whereas exclusive carotenoid peaks were traced at 456 nm, as shown in Fig. 4. The whole cell extract yielded a distinctive peak corresponding to zeaxanthin (Zea) (see Fig. 4, *A* and *B*), which nearly equalled the main Chl*a* peak (see Fig. 4*A*). In contrast, the amount of β-carotene was 3-fold lower compared with Chl*a*

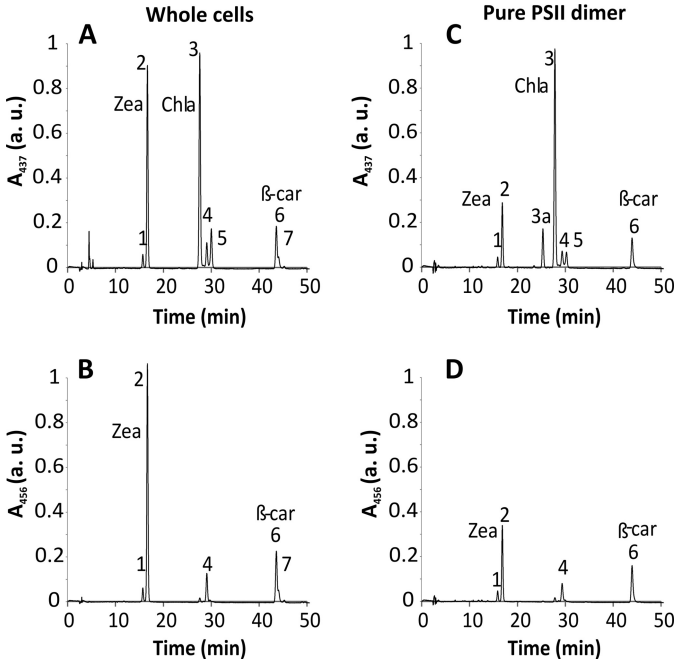

FIGURE 4. **HPLC pigment analysis of *C. merolae* cells and PSII dimer.** Total pigments were analyzed by HPLC, and their absorbance was measured at 437 nm (for carotenoids and Chl*a*) and at 456 nm (for carotenoids only). Peak identities are as follows. *1*, Zea (*cis* isomer); *2*, Zea; *3a*, oxidized Chl*a*; *3*, Chl*a*; *4*, β-cryptoxanthin; *5*, Chl*a*′; *6*, β-carotene; *7*, β-carotene (*cis* isomer). Peaks were assigned to the corresponding pigments by LC-MS according to Ref. 39. Whole cell extract yielded a distinctive peak corresponding to Zea (*A* and *B*) nearly identical to the peak of Chl*a* (*A*), whereas the β-carotene peak was 3-fold lower than that of Chl*a*. The Zea abundance in the pure PSII dimer was significantly lower than in whole cells (*C*); however, the relative contribution of Zea and β-carotene was similar (*D*) when PSII was compared with the whole cell extract (see Table 1). *a.u.*, arbitrary units.

TABLE 1

Relative abundance of zeaxanthin and β-carotene in whole cells and purified PSII

Molar ratios of pigments were calculated by integration of an area underneath the relevant peak and using extinction coefficients, as described under "Materials and Methods." S.D. values were calculated from two independent measurements ($n = 2$).

Source	Zea/Chl*a*	Zea/β-carotene	β-Carotene/Chl*a*
PSII	0.275 ± 0.033	2.140 ± 0.270	0.131 ± 0.015
Intact cells	0.880 ± 0.033	4.230 ± 0.180	0.210 ± 0.007

(Fig. 4*A*). The level of Zea in the pure PSII dimer was 3-fold lower compared with the whole cells (Fig. 4, compare *A* and *C*), whereas the relative ratio of Zea to β-carotene was 2-fold lower in the purified PSII dimer compared with the whole cells (Fig. 4, compare *B* and *D*; see Table 1). We did not detect any peaks corresponding to violaxanthin or antheraxanthin, either in the whole cells or in the purified PSII.

Investigation into the in Vivo and in Vitro Photoprotection Mechanisms in C. merolae—In order to gain an insight into the photoprotective mechanisms in *C. merolae*, we set out to dissect the locus of NPQ both *in vivo* (intact cells) and *in vitro* (isolated PSII dimers). We investigated the presence and extent of photoprotective NPQ *in vivo* by measuring the variable Chl*a* fluorescence (F_V) in intact *C. merolae* cells (Fig. 5). A typical measuring protocol has been applied to exclude the effect of state transitions on the maximal fluorescence in dark (F_M) that is known to be affected by the phycobilisome binding in cyano-

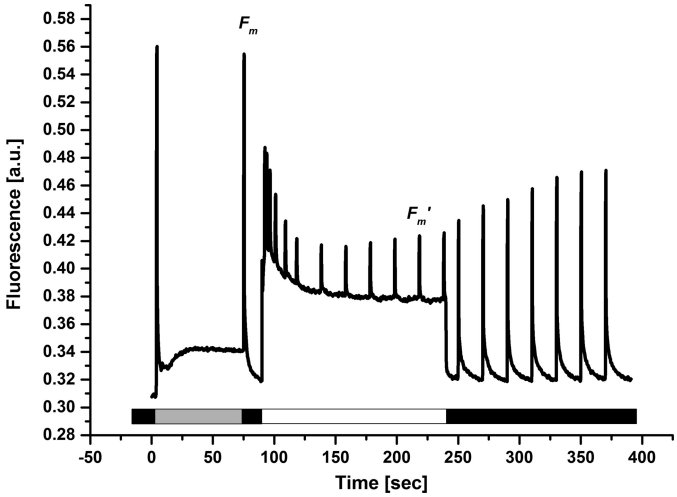

FIGURE 5. **Fluorescence quenching in *C. merolae* cells exposed to blue light.** Cells were adapted for 20 min in the dark and then used for *in vivo* measurements of NPQ. Low intensity blue light was used (~7 μE/m²/s; *dark gray bar*) to reach maximal fluorescence in the dark (F_M). Quenching of maximal fluorescence upon high intensity blue light exposure (750 μE/m²/s; *white bar*) and its recovery in the dark (*black bar*) were observed. The NPQ value was calculated based on the Stern-Volmer formula, $(F_M - F_M')/F_M'$. *a.u.*, arbitrary units.

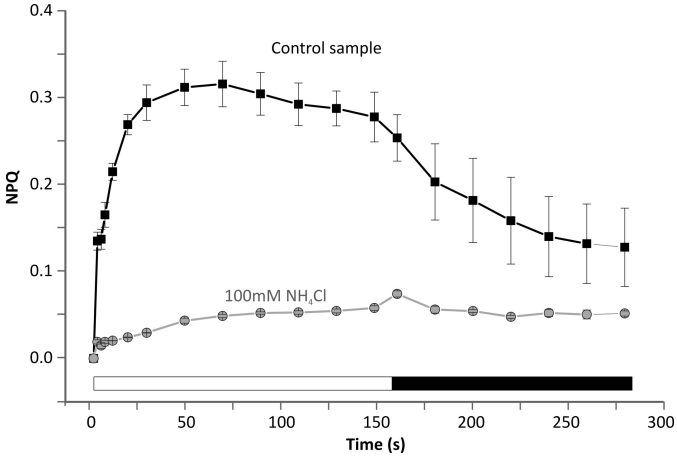

FIGURE 6. **Non-photochemical quenching kinetics in *C. merolae* cells.** The induction of NPQ was measured in dark-adapted cells exposed to blue light (750 μE/m²/s; *white bar*) followed by recovery in the dark (*black bar*). Curves were measured either without any inhibitors (control sample) or after the addition of an uncoupler (100 mM NH_4Cl) that disrupts lumen acidification. Data represent averages and S.D. (*error bars*) for $n = 3$.

bacteria (54). There were no significant changes in the F_M value after a short period of illumination with low intensity blue light, excluding the putative influence of state transitions on the measured F_M values. The F_M value obtained in the dark (see Fig. 5) was then used for calculation of the NPQ kinetics upon transition of the cells to light (Fig. 6). The exposure of dark-adapted *C. merolae* cells to high intensity blue light resulted in pronounced quenching of maximal fluorescence (F_M'), in a process that was reversible in the dark (see Fig. 5). These results confirmed the presence of NPQ in *C. merolae* cells *in vivo*. Maximal NPQ value was around 0.4 (Fig. 6), and resembled the value determined for cyanobacteria (54), indicating a similar amount of energy that is dissipated during NPQ despite different quenchers employed by both phototrophs. The NPQ was inhibited *in vivo* after the addition of an uncoupler NH_4Cl (Fig. 6),

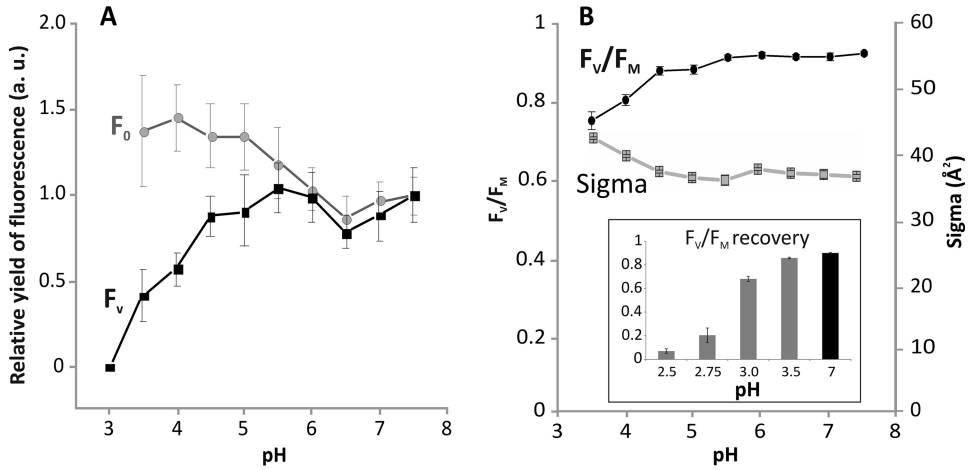

FIGURE 7. **Dissection of the NPQ locus in *C. merolae* PSII.** *A*, relative yields of minimal (F_0) and variable fluorescence (F_V) of isolated PSII as a function of pH. Values represent averages and S.D. values from six measurements ($n = 6$) done with two independent PSII isolations. Data are normalized to fluorescence parameters at pH 7.5. For pH 3 and lower, there was no detectable variable fluorescence; therefore, other physiological parameters indicating closed (F_M) or opened (F_0) RC were calculated only in the pH range 3.5–7.5. *B*, maximal quantum yield (F_V/F_M) and effective antennae size (σ_{PSII}) of isolated PSII as a function of pH. Values represent averages and S.D. values from six measurements ($n = 6$) done with two independent PSII preparations. *Inset*, reversibility of PSII efficiency (F_V/F_M) after a treatment with low pH. All values were measured at pH 7, either after 2-min treatment at low pH (2.5–3.5) followed by 4 min of recovery at pH 7 (*gray bars*) or directly at pH 7 without prior low pH treatment (*black bar*). Data represent averages and S.D. (*error bars*) for $n = 3$. *a.u.*, arbitrary units.

demonstrating the role of acidification of the lumen in triggering NPQ in *C. merolae* cells.

In order to gain the first glimpse into the mechanism of photoprotection in isolated *C. merolae* dimeric PSII complexes, we measured the effect of various pH levels (pH range of 3–7.5) on variable Chl*a* fluorescence, F_V. Photoprotective NPQ that is triggered by low pH can be demonstrated by detection of a decrease of F_V (see Ref. 29 for a recent review). As shown in Fig. 7*A*, variable fluorescence of PSII was progressively reduced at pH below 4.5 and completely disappeared at pH 3. This F_V decrease was correlated with the reduction of maximal PSII efficiency, F_V/F_M (see Fig. 7*B*), and with a decrease of the oxygen evolution rate at this pH range (compare Figs. 3*A* and 7). These data indicate that the reduction of photochemical PSII efficiency at low pH is due to stimulation of non-photochemical pathways of de-excitation. In contrast to the pH-dependent F_V decrease, there was no quenching of minimal fluorescence (F_0) at low pH (see Fig. 7*A*). Because we have not found any external LHC-type antennae attached to the isolated PSII dimers (see supplemental Table S1), this selective quenching of variable fluorescence (F_V) suggests the presence of the NPQ locus in the *C. merolae* PSII reaction center. A similar mechanism has been proposed for PSII isolated from higher plants (35, 36).

We observed a clear reversibility of low pH-induced changes in maximal PSII efficiency F_V/F_M, upon transfer of PSII from low to neutral pH. The maximal efficiency of PSII almost fully recovered upon transfer from pH 3.5, with almost 70% recovery of the F_V/F_M ratio following incubation of PSII at pH 3 (see Fig. 7*B*, *inset*), at which no variable fluorescence F_V was observed (Fig. 7*A*). These data clearly confirm the presence of reversible photoprotective NPQ in the dimeric *C. merolae* PSII exposed to extreme low pH. No NPQ was observed when PSII was exposed to pH below 3 (see Fig. 7*B*, *inset*), most likely due to the irreversible damage to the OEC on the donor side and denaturation of the PSII complex. We have tested correlation between low pH-induced changes in F_M and inhibition of oxygen evolution

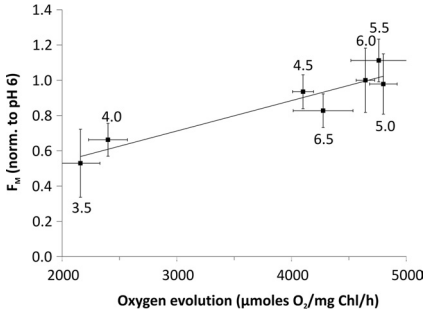

FIGURE 8. **Correlation between low pH induced maximal fluorescence quenching and inhibition of oxygen evolution in the isolated *C. merolae* PSII.** Values of F_M were normalized at pH 6 and plotted with values of PSII activity at a given pH (numerical values by the data points). A linear correlation with the correlation factor $R^2 = 0.89$ ($p = 0.0014$) of both data sets was observed, indicating that within the pH range of 3.5–6.5, the loss of activity is related to quenching of fluorescence and not to irreversible damage to OEC. No such correlation was observed at pH 7 and 7.5. *Error bars*, S.D.

TABLE 2

Effective PSII antennae size (σPSII) in intact *C. merolae* cells and isolated PSII

Values represent averages and S.D. from six measurements ($n = 6$) done with two independent PSII isolations.

Source	Intact cells	Thylakoids	PSII (pH 6)	PSII (pH 3.5)
σ_{PSII}	52.8 ± 1.6	38.1 ± 0.7	37.1 ± 0.9	41.8 ± 1.3

rates. We observed linear correlation between F_M quenching and reduction in oxygen evolution rates at low pH (pH 3.5–6.5) (see Fig. 8). Conversely, no such correlation was observed at higher pH (pH 7 and 7.5), when the O_2 evolution rate was reduced, whereas F_M remained non-quenched (see Figs. 3*A* and 7*A*). This is in line with the fact that only low pH can trigger NPQ *in vivo*.

We further explored the mechanism of NPQ in *C. merolae* PSII by measuring the effective antennae size of PSII (σ_{PSII}) corresponding to the inner antenna Chls (see Table 2). In intact *C. merolae* cells, the antennae size of PSII was ~30% higher compared with isolated thylakoid membranes or dimeric

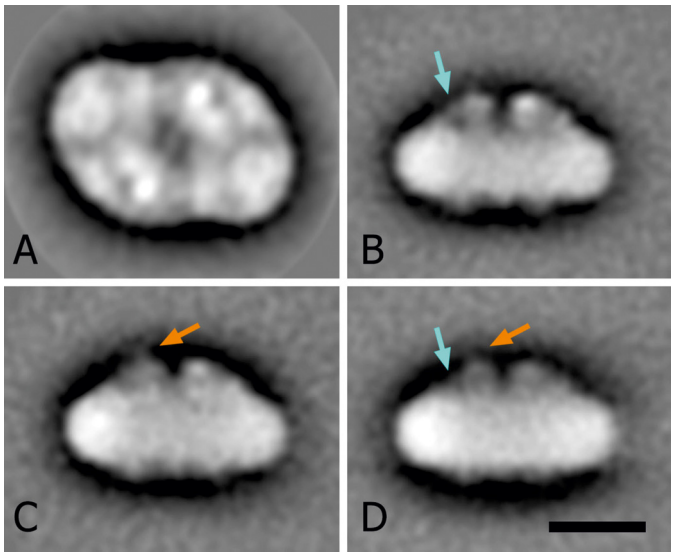

FIGURE 9. **Projection maps of the *top* and *side views* of *C. merolae*.** *A*, final projection map of the *top view*, as seen from the lumenal side of the membrane; the sum is composed of the best 2,048 particles, according to their correlation coefficient in the last alignment step. Two-fold rotational symmetry was imposed after analysis. *B–D*, averaged images of three classes of *side views*. The sums are composed of 493, 588, and 353 projections, respectively. As a main difference between the classes, the *orange arrows* indicate a stronger (*C*) or fainter (*D*) presence of the 12-kDa subunit on top of the other extrinsic subunits. *Blue arrows* show a stronger (*B*) and weaker (*D*) visibility of the cytochrome c_{550} subunit. *Scale bar* (*A–D*), 10 nm.

PSII complexes, indicating a partial loss in delivering excitation energy to PSII upon solubilization of this complex from the membranes. Because the effective antennae size of the *C. merolae* PSII was similar to that observed for the higher plant complex (see Ref. 36), our PSII dimer was isolated in a fully native and functional form. There was no significant difference in σ_{PSII} for isolated PSII and thylakoids that contain both PSI and PSII (see Table 2). In isolated PSII, we did not observe any decrease of σ_{PSII} at pH 3.5, a pH value at which F_V was already significantly reduced (Fig. 7, compare *A* and *B*). The constant (or slightly increasing) values of σ_{PSII} at low pH preclude the possibility of de-excitation of excess light occurring within the internal PSII-core antennae CP43 and CP47 because such a mechanism would imply a decrease in both σ_{PSII} and F_V.

Structural Analysis of the C. merolae PSII Dimer—In order to get an impression of subunit organization within the *C. merolae* PSII dimer, we visualized the complex by negative stain electron microscopy combined with single particle analyses. Single particle averaging of a large set of dimers showed that the particles were mostly present in top lumenal or side view positions. Within the top views, there was little variation, allowing for the final projection map to be obtained at a resolution of 17 Å, as depicted in Fig. 9*A*. In the class of side view projections, we detected some variation at the site of the extrinsic subunits, which resulted in a partition of the data set into three classes (Fig. 9, *B–D*). As a main difference between the classes, there is a stronger or fainter presence of the 12-kDa subunit (PsbU) at the top of the other extrinsic subunits (*orange arrows* in Fig. 9, *C* and *D*). In addition, the visibility of the cytochrome c_{550} (PsbV) subunit is variable (*blue arrows* in Fig. 9, *B* and *D*), despite the apparent 1:1 stoichiometry of PsbV/PSII (data not shown). The size of a side view *C. merolae* PSII dimer particle (Fig. 9, *B–D*) was estimated at 21.2 × 11 nm, which is in a good agreement with the size of the PSII dimers isolated from another red alga, *P. cruentum* (49), as well as dimensions of the cyanobacterial PSII dimer calculated from the atomic crystal structure (19.9 × 11.6 nm; see Ref. 1).

Comparison with the structural work on cyanobacterial PSII dimers could give us a hint of where PsbQ′, an extra extrinsic subunit of *C. merolae* over and above the cyanobacterial homologues (PsbO, PsbU, and PsbV), is located. First, the side views were analyzed because in this position we observed less overlap between the PSII subunits, allowing for the distinctive differences between the maps to be dissected. Indeed, we identified an additional protein mass visible in the map of *C. merolae* (Fig. 10*A*) compared with the high resolution structure of PSII from *T. vulcanus* (Fig. 10*B*) digitally truncated to 8 Å for comparison of protein densities. The *yellow asterisk* indicates the position where the *C. merolae* PSII dimer seems to have protein mass that is absent in the cyanobacterial structure (Fig. 10, compare *A* and *B*). The most obvious candidate for the location in this position is the additional lumenal extrinsic subunit PsbQ′.

DISCUSSION

In the present work, we isolated and purified the dimeric PSII complex from the red alga *C. merolae* and demonstrated its remarkable robustness over a range of extreme conditions, including high light illumination, high temperatures, and extreme pH range conditions that usually lead to destablization of the OEC and inhibition of PSII function. The oxygen-evolving activity of the isolated complex is one of the highest reported to date and exceeds the activity of dimeric PSII complexes isolated from, for example, the thermophilic cyanobacteria *T. elongatus* and *T. vulcanus* used to obtain medium to high resolution structures of PSII (1, 2, 53). Although the pH optimum for the activity of the *C. merolae* PSII complex is at pH 5–5.5, the complex sustains over 40–60% of its oxygen-evolving activity at pH 3.5 and pH 7, which is unprecendented for other PSII preparations isolated from thermophilic cyanobacteria (55–57), mesophylic and other thermoacidophilic red algae (38, 49), green algae (58), and higher plants (59, 60). Moreover, the *C. merolae* complex increases its activity at relatively high temperatures up to 45 °C as well as retaining its intactness over a prolonged period of incubation at room temperatures (see Fig. 3), which may make this complex amenable to application in biomimetic solar-to-fuel devices often intended to operate at elevated temperatures over extended periods of time (61, 62).

One important question arises: what are the molecular mechanisms responsible for the remarkable robustness of *C. merolae* PSII, especially under extreme illumination conditions? Under the conditions of imbalance between energy capture and utilization (*e.g.* in high light), accumulation of excitons in external and intrinsic antennae of both photosystems increases the occurrence of singlet Chl-excited states (^{1}Chl*). Under excess light, ^{1}Chl* species often undergo intersystem crossing to form the Chl triplet state (^{3}Chl*) (63). This species reacts with molecular oxygen to form highly reactive oxygen species, including singlet oxygen ($^1O_2$), when excitations are not rapidly quenched. This can occur when the capacity for productive photochemical quenching is exceeded and non-

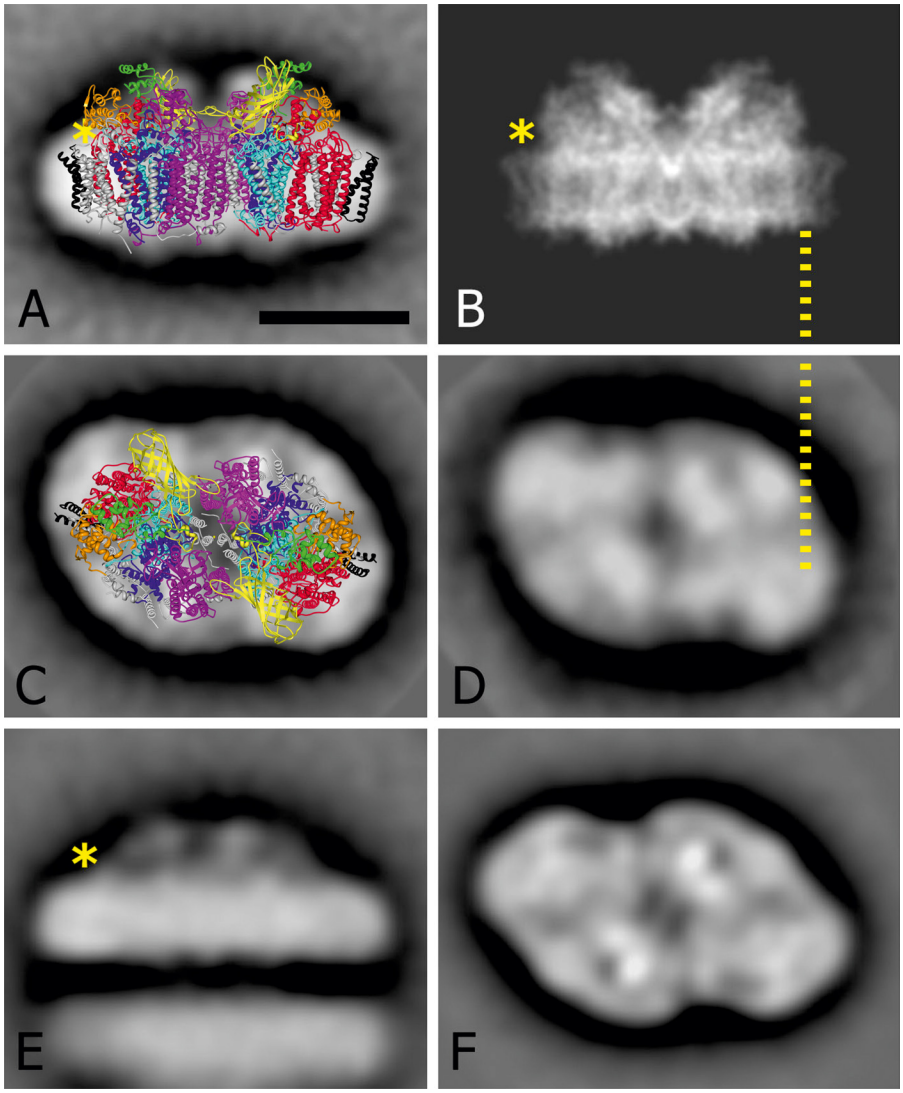

FIGURE 10. **Comparison of dimeric PSII projection maps to visualize differences between *C. merolae* and *T. elongatus* at the subunit level.** *A* and *C*, *side* and *lumenal top view* projection maps of the *C. merolae* PSII dimer particles, respectively. In *A*, the 1.9 Å structure of PSII from *T. vulcanus* (1) (Protein Data Bank coordinates 3ARC) was overlaid onto the *top view* EM projection map of the *C. merolae* complex. The D1 (PsbA) and D2 (PsbD) subunits are *colored* in *light blue* and *dark blue*, respectively. The CP43 (PsbC) and CP47 (PsbB) subunits are depicted in *red* and *magenta*, respectively. The PsbZ subunit is *highlighted* in *black*. The extrinsic subunits PsbV, PsbU, and PsbO are shown in *orange*, *green*, and *yellow*, respectively. For clarity, all remaining subunits are shown in *gray*. The overall size of PSII dimer particles in *A* is 21.2 × 11 nm. *B*, a high resolution structure of *T. vulcanus* PSII seen from aside and truncated at 8 Å resolution (1). *D* and *E*, *top* and *side views* of *T. elongatus* PsbZ-less PSII dimers (82); *F*, *top view* of *T. elongatus* PSII containing PsbZ (83). The *dotted line* correlates the position of an additional density with the CP43 subunit in the *side view map* (*B*) and in the *top view* (*D*). *, location where PsbQ′ is located in the *C. merolae* PSII complex and is absent in the *T. vulcanus* and the *T. elongatus* complex. *Scale bar*, 10 nm.

photochemical quenching is insufficient or not yet sufficiently turned on (64–66).

Our carotenoid and chlorophyll fluorescence quenching analyses point to the involvement of both zeaxanthin and the primary oxidant, $P680^+$, being responsible for the photoprotection of thylakoids and PSII under high light irradiance. It is well established that carotenoids are essential for photoprotection in oxygenic photosynthesis (reviewed in Refs. 28, 63, 67, and 68). Moreover, they affect assembly and stability of the PSII reaction center and light-harvesting antenna subunits (69, 70).

Of all of the carotenoids, Zea plays a particularly important role in photoprotection. High light-induced synthesis of Zea and its binding to the specific proteins enhance photoprotection by decreasing the yield of potentially dangerous Chl-excited states. A recent study using time-resolved differencial spectroscopy demonstrated increased efficiency of this molecule in controlling ^{3}Chl* species formation (71). Zea is known to be involved in several types of photoprotection of the PSII reaction centers that occur at various time scales: (i) rapid feedback de-excitation quenching (qE) of ^{1}Chl*, (ii) a slowly inducible quenching (qZ) caused by Zea binding to LHC upon exchange with violaxanthin, and (iii) a long term irreversible quenching associated with PSII photoinhibition (71).

In this work, we have identified a considerable amount of Zea both in intact *C. merolae* cells and in the isolated PSII complex (see Fig. 4 and Table 1), indicating that this xanthophyll may play an important photoprotective role in reactive oxygen species scavenging in the lipid phase of *C. merolae* thylakoids. Because the light-harvesting antenna of red algal PSII is formed by phycobilisomes, it is unlikely that Zea would be involved in

slowly inducible quenching qZ. Importantly, our pigment quantification suggests that in the *C. merolae* PSII complex, Zea may also be present inside the PSII core complex, where it may take a direct role in quenching of ^{3}Chl* species. Taking into account the pigment molar ratios presented in Table 1 and normalizing these values to 35 Chl*a* molecules/PSII, as determined in the latest atomic structure (1), we estimate 4–5 β-carotenes and 8–10 Zea molecules in our PSII complex. Because we would expect 11 β-carotenes/PSII (1), it is possible that Zea may replace some β-carotenes in the *C. merolae* PSII complex, perhaps at the boundary of CP43 and associated low molecular weight subunits. This intriguing possibility needs to be supported by a more detailed study.

Our present data showing insensitivity of the effective PSII antennae size to low pH-induced quenching (Fig. 7*B*) seems to exclude a direct role of *C. merolae* PSII inner antennae in quenching. The pH insensitivity of the effective antennae size during NPQ is characteristic of the NPQ locus present within the closed reaction centers upon charge recombination (34, 72). It is therefore possible that some Zea molecules putatively bound in the vicinity of the charge separation pathway in *C. merolae* PSII could be involved in the RC-based quenching observed in the present study. Similarly, Fleming and colleagues (73) observed that the mechanism of non-radiative deactivation of ^{1}Chl* during excess light occurs by excitation transfer to a Chl-Zea heterodimer, followed by ultrafast $Car^{+\cdot}$ formation. Such a process was observed for Zea bound within the peripheral light-harvesting antenna of PSII. Whether a similar mechanism exists for Zea putatively bound within the RC of red algal PSII remains to be elucidated.

Alternatively, Zea could play a direct antioxidant role in scavenging free radicals and singlet oxygen molecules produced in high light in the lipid phase of the thylakoid membrane in the vicinity of PSII macrodomains (74). In light of the high lipid content of the cyanobacterial PSII dimer shown in its latest atomic structure (1), it is tempting to speculate that free Zea molecules bound within the *C. merolae* PSII complex-lipid interface may protect these intrinsic lipid molecules from $^1O_2$-mediated peroxidation. A similar NPQ-independent protective role of Zea in scavenging singlet oxygen has been observed for the *ch1* mutant of *Arabidopsis thaliana* devoid of the LHCII antenna (75). In addition, Zea identified in this study in intact cells of *C. merolae* might play a role as a thylakoid membrane-rigidifying molecule (76, 77), allowing this extremophilic alga to thrive at high temperatures.

Similarly, Gantt and colleagues (78) showed that in another unicellular red alga, *P. cruentum*, the cellular content of Zea increased with growth irradiance, confirming a role for this carotenoid in photoprotection. In the latter work, the ratio of cellular Zea/β-carotene incrementally increased upon high light exposure of *Porphyridium* cells and was similar to the ratio obtained in this study for similar conditions of illumination (2.6 and 2.8, respectively). The relative content and composition of carotenoids and Chl are also similar in *C. merolae* (see Table 1 in this study and Ref. 39) and *P. cruentum* cells (78). Importantly, we did not detect violaxanthin either in whole cells or purified PSII (see Fig. 4) and PSI (not shown), confirming the previous data of Gantt and colleagues (39), who showed that this dieepoxide xanthophyll is absent in *C. merolae* cells. Instead, in this organism, Zea most likely forms by conversion of β-carotene via intermediate β-cryptoxanthin (79), a process catalyzed by β-carotene 3-hydroxylase enzymes, such as the CrtR cyanobacterial type β-carotene hydroxylase or cytochrome P450 (39).

In addition to the Zea-mediated photoprotection, our fluorescence measurements clearly point to the pH-dependent reaction center quenching as the main photoprotective mechanism in the *C. merolae* PSII. This type of quenching seems to sustain a high oxygen-evolving activity of *C. merolae* PSII even at extremely high irradiation (see Fig. 3). Kirilovsky and colleagues (32, 33) have shown that non-photochemical quenching in mesophilic red algae is triggered by low pH and may occur in the PSII reaction center rather than the inner antenna. However, a direct proof for this type of photoprotective mechanism and dissection of its exact locus were missing because their work was performed exclusively in intact cells. Due to this limited experimental approach, the authors could only suggest the reaction center-based mechanism of NPQ in red algae based on indirect measurements of F_0 pH insensitivity during stimulation of non-photochemical quenching (32, 33).

Here, we provide the first direct evidence of the PSII reaction center as the primary locus of pH-dependent NPQ in the extremophilic red algae. This type of quenching can occur through (i) energy dissipation via alternative electron transport after primary radical pair production, (ii) charge recombination between $Pheo^-$ and $P680^+$ (80), (iii) rapid charge recombination between Q_{A^-} and $P680^+$, and (iiii) accumulation of $P680^+$ that can act as a direct quencher (30, 36). All four types of RC-based quenching are consistent with pH insensitivity of effective antenna size during quenching. Indeed, our measurements of the absorbance cross-section of isolated *C. merolae* PSII revealed no decrease in the functional antenna size at low pH (see Fig. 7*B*), which supports a reaction center-based quenching mechanism in this extremophile when exposed to saturating light levels. Importantly, we detected significantly decreased F_V values at low pH, a phenomenon that was rapidly reversible upon exposure of PSII to physiological pH (see Fig. 7*B*). We also observed a significant correlation between F_M (and F_V) quenching and inhibition of oxygen evolution in isolated PSII at low pH (see Fig. 8) and a lack thereof at higher pH. These data exclude the possibility of the OEC inactivation as the primary cause for fluorescence quenching in the isolated *C. merolae* PSII and confirm the presence of reversible low pH-induced NPQ in this complex.

We previously obtained three-dimensional crystals of the *C. merolae* PSII dimer (81) with the aim of solving the structure of this complex. Because we were unable to significantly improve the resolution of x-ray diffraction patterns obtained from these crystals, we applied electron microscopy coupled with single particle analyses of the isolated PSII dimer to gain an insight into the structure of this eukaryotic complex, in particular its lumenal side. Comparison with structural work on cyanobacterial PSII dimers allowed us to suggest an assignment of the position for the PsbQ′, an extra extrinsic subunit over and above the cyanobacterial-like PsbO, PsbU, and PsbV subunits stabilizing the OEC in the *C. merolae* complex (24–26). In our

difference map in which the atomic structure of cyanobacterial PSII was modeled onto the averaged side and lumenal top view projections of the *C. merolae* PSII dimer particles, the additional density attributed to PsbQ′ is present close to the lumenal side of the membrane, in the vicinity of the CP43 inner antenna subunit (see Fig. 10). Our assignment of the PsbQ′ position is supported by previous EM studies of cyanobacterial PSII (82, 83), whereby the side view dimer projection lacks the additional mass identified in our *C. merolae* PSII dimer particles (Fig. 10*E*). Another position would be in the center, because the EM and x-ray data also differ here, such that in the EM map, the extrinsic protein densities for both monomers appear to be more compact. However, this location is unlikely, because the cyanobacterial map of *T. elongatus* is essentially the same in this position (Fig. 10*E*).

Our assignment of PsbQ′ differs somewhat from that presented for the dimeric PSII particles from a closely related red alga, *C. caldarium* (22), in that it places this additional OEC subunit closer to the membrane in the vicinity of the CP43 intrinsic antenna subunit. Vacha and colleagues proposed positioning of PsbQ′ more toward the lumenal space, between the PsbU and PsbV subunits (22). However, in contrast to the present work, they were unable to reveal any additional protein densities in the projection maps of *C. caldarium* compared with the equivalent maps of *P. cruentum* (49) and *T. elongatus* (82) PSII dimer particles.

The comparison with the cyanobacterial data further shows a surprising similarity between the top lumenal views of both *C. merolae* (Fig. 10*C*) and *T. elongatus* (Fig. 10*D*). There are no significant differences in surface densities, indicating that the extra subunit of *C. merolae* is not visible, most likely due to an overlap with the membrane-integrated moiety of the PSII dimer, possibly the CP43 intrinsic antenna subunit. The close similarity in the surface and shape points to a highly similar composition of the membrane-bound subunits. The map, as depicted in Fig. 10*D*, was obtained from a PSII particle lacking the PsbZ protein. This protein was, however, present in the map shown in Fig. 10*F* (83). Thus, it seems that our *C. merolae* PSII particles do not contain a subunit homologous to the cyanobacterial PsbZ subunit. Interestingly, in the side view projection map of the *C. merolae* PSII dimer, the position of the PsbO subunit seems to be slightly shifted toward the pseudosymmetry axis of the dimer, compared with the crystal structure of the cyanobacterial counterpart (see Fig. 10*A*). A similar phenomenon was observed for subpopulations of the dimeric PSII from a green alga *Chlamydomonas reinhardtii* with altered organization of the LHCII antenna,[4] suggesting a certain level of structural flexibility within the OEC region.

Interestingly, our mass spectrometry analysis showed the presence of the PSII auxiliary subunit Psb27 and a low molecular weight subunit PsbW implied in the regulation of the PSII repair cycle (84) and stabilization of the PSII dimers in higher plants (85). Both proteins were detected in all rounds of MS/MS analysis from three independent preparations, suggesting their stable association with the population of *C. merolae* PSII (probably in its inactive form), which most likely undergoes a repair cycle. However, the stoichiometry of their binding to PSII as well as the turnover rate for the *C. merolae* PSII are presently unknown and will be a subject of future studies.

[4] M. Webber-Birungi, B. Drop, S. Yadav, R. Croce, and E. J. Boekema, unpublished data.

Acknowledgment—We thank A. K. Jagielski (Department of Metabolic Regulation, Faculty of Biology, University of Warsaw) for assistance in mass spectrometry data collection.

REFERENCES

1. Umena, Y., Kawakami, K., Shen, J. R., and Kamiya, N. (2011) Crystal structure of oxygen-evolving photosystem II at a resolution of 1.9 Å. *Nature* **473,** 55–60
2. Ferreira, K. N., Iverson, T. M., Maghlaoui, K., Barber, J., and Iwata, S. (2004) Architecture of the photosynthetic oxygen-evolving center. *Science* **303,** 1831–1838
3. Kargul, J., Maghlaoui, K., Murray, J. W., Deak, Z., Boussac, A., Rutherford, A. W., Vass, I., and Barber, J. (2007) Purification, crystallization and X-ray diffraction analyses of the *T. elongatus* PSII core dimer with strontium replacing calcium in the oxygen-evolving complex. *Biochim. Biophys. Acta* **1767,** 404–413
4. Murray, J. W., Maghlaoui, K., Kargul, J., Ishida, N., Lai, T.-L., Rutherford, A. W., Sugiura, M., Boussac, A., and Barber, J. (2008) X-ray crystallography identifies two chloride binding sites in the oxygen evolving centre of Photosystem II. *Energy Environ. Sci.* **1,** 161–166
5. Murray, J. W., Maghlaoui, K., Kargul, J., Sugiura, M., and Barber, J. (2008) Analysis of xenon binding to photosystem II by x-ray crystallography. *Photosynth. Res.* **98,** 523–527
6. Kamiya, N., and Shen, J. R. (2003) Crystal structure of oxygen-evolving photosystem II from *Thermosynechococcus vulcanus* at 3.7-Å resolution. *Proc. Natl. Acad. Sci.* **100,** 98–103
7. Loll, B., Kern, J., Saenger, W., Zouni, A., and Biesiadka, J. (2005) Towards complete cofactor arrangement in the 3.0 Å resolution structure of photosystem II. *Nature* **438,** 1040–1044
8. Guskov, A., Kern, J., Gabdulkhakov, A., Broser, M., Zouni, A., and Saenger, W. (2009) Cyanobacterial photosystem II at 2.9-Å resolution and the role of quinones, lipids, channels and chloride. *Nat. Struct. Mol. Biol.* **16,** 334–342
9. Yano, J., Kern, J., Sauer, K., Latimer, M. J., Pushkar, Y., Biesiadka, J., Loll, B., Saenger, W., Messinger, J., Zouni, A., and Yachandra, V. K. (2006) Where water is oxidized to dioxygen. Structure of the photosynthetic Mn_4Ca cluster. *Science* **314,** 821–825
10. Sproviero, E. M., Shinopoulos, K., Gascón, J. A., McEvoy, J. P., Brudvig, G. W., and Batista, V. S. (2008) QM/MM computational studies of substrate water binding to the oxygen-evolving centre of photosystem II. *Philos. Trans. R. Soc. Lond. B Biol. Sci.* **363,** 1149–1156
11. Dau, H., Grundmeier, A., Loja, P., and Haumann, M. (2008) On the structure of the manganese complex of photosystem II. Extended-range EXAFS data and specific atomic-resolution models for four S-states. *Philos. Trans. R. Soc. Lond. B Biol. Sci.* **363,** 1237–1243; discussion 1243–1244
12. Cox, N., and Messinger, J. (2013) Reflections on substrate water and dioxygen formation. *Biochim. Biophys. Acta*, in press
13. Siegbahn, P. E. (2013) Water oxidation mechanism in photosystem II, including oxidations, proton release pathways, O—O bond formation and O_2 release. *Biochim. Biophys. Acta*, in press
14. Badura, A., Esper, B., Ataka, K., Grunwald, C., Wöll, C., Kuhlmann, J., Heberle, J., and Rögner, M. (2006) Light-driven water splitting for (bio-)hydrogen production. Photosystem II as the central part of a bioelectrochemical device. *Photochem. Photobiol.* **82,** 1385–1390
15. Vittadello, M., Gorbunov, M. Y., Mastrogiovanni, D. T., Wielunski, L. S., Garfunkel, E. L., Guerrero, F., Kirilovsky, D., Sugiura, M., Rutherford, A. W., Safari, A., and Falkowski, P. G. (2010) Photoelectron generation by photosystem II core complexes tethered to gold surfaces. *ChemSusChem* **3,** 471–475
16. Kato, M., Cardona, T., Rutherford, A. W., and Reisner, E. (2012) Photo-

electrochemical water oxidation with photosystem II integrated in a mesoporous indium-tin oxide electrode. *J. Am. Chem. Soc.* **134,** 8332–8335
17. Barber, J., and Tran, P. D. (2013) From natural to artificial photosynthesis. *J. R. Soc. Interface* **10,** 20120984
18. Ciniglia, C., Yoon, H. S., Pollio, A., Pinto, G., and Bhattacharya, D. (2004) Hidden biodiversity of the extremophilic *Cyanidiales* red algae. *Mol. Ecol.* **13,** 1827–1838
19. Enami, I., Adachi, H., and Shen, J.-R. (2010) Mechanisms of acido-tolerance and characteristics of photosystems in an acidophilic and thermophilic red alga, *Cyanidium caldarium.* in *Red Algae in the Genomic Age* (Seckbach, J., and Chapman, D. J., eds) pp. 375–389, Springer, Dordrecht, The Netherlands
20. Nozaki, H., Matsuzaki, M., Takahara, M., Misumi, O., Kuroiwa, H., Hasegawa, M., Shin-i, T., Kohara, Y., Ogasawara, N., and Kuroiwa, T. (2003) The phylogenetic position of red algae revealed by multiple nuclear genes from mitochondria-containing eukaryotes and an alternative hypothesis on the origin of plastids. *J. Mol. Evol.* **56,** 485–497
21. Wolfe, G. R., Cunningham, F. X., Durnford, D., Green, B. R., and Gantt, E. (1994) Evidence for a common origin of chloroplasts with light-harvesting complexes of different pigmentation. *Nature* **367,** 566–568
22. Gardian, Z., Bumba, L., Schrofel, A., Herbstova, M., Nebesarova, J., and Vacha, F. (2007) Organisation of photosystem I and photosystem II in red alga *Cyanidium caldarium*. Encounter of cyanobacterial and higher plant concepts. *Biochim. Biophys. Acta* **1767,** 725–731
23. Busch, A., Nield, J., and Hippler, M. (2010) The composition and structure of photosystem I-associated antenna from *Cyanidioschyzon merolae*. *Plant J.* **62,** 886–897
24. Ohta, H., Suzuki, T., Ueno, M., Okumura, A., Yoshihara, S., Shen, J.-R., and Enami, I. (2003) Extrinsic proteins of photosystem II. An intermediate member of PsbQ protein family in red algal PSII. *Eur. J. Biochem.* **270,** 4156–4163
25. Enami, I., Kikuchi, S., Fukuda, T., Ohta, H., and Shen, J. R. (1998) Binding and functional properties of four extrinsic proteins of photosystem II from a red alga, *Cyanidium caldarium*, as studied by release-reconstitution experiments. *Biochemistry* **37,** 2787–2793
26. Bricker, T. M., Roose, J. L., Fagerlund, R. D., Frankel, L. K., and Eaton-Rye, J. J. (2012) The extrinsic proteins of photosystem II. *Biochim. Biophys. Acta* **1817,** 121–142
27. Kargul, J., and Barber, J. (2008) Photosynthetic acclimation. Structural reorganisation of light harvesting antenna. Role of redox-dependent phosphorylation of major and minor chlorophyll *a*/*b* binding proteins. *FEBS J.* **275,** 1056–1068
28. Horton, P., Johnson, M. P., Perez-Bueno, M. L., Kiss, A. Z., and Ruban, A. V. (2008) Photosynthetic acclimation. Does the dynamic structure and macro-organisation of photosystem II in higher plant grana membranes regulate light harvesting states? *FEBS J.* **275,** 1069–1079
29. Ruban, A. V., Johnson, M. P., and Duffy, C. D. (2012) The photoprotective molecular switch in the photosystem II antenna. *Biochim. Biophys. Acta* **1817,** 167–181
30. Ivanov, A. G., Sane, P. V., Hurry, V., Oquist, G., and Huner, N. P. (2008) Photosystem II reaction centre quenching. Mechanisms and physiological role. *Photosynth. Res.* **98,** 565–574
31. Kirilovsky, D., Kaňa, R., and Prášil, O. (2013) Mechanisms modulating energy arriving at reaction centers in cyanobacteria. in *Non-photochemical Quenching and Thermal Energy Dissipation in Plants, Algae and Cyanobacteria* (Demmig-Adams, B., Adams, W., Garab, G., and Govindjee, eds) Springer, Netherlands, Dordrecht, in press
32. Delphin, E., Duval, J. C., Etienne, A. L., and Kirilovsky, D. (1996) State transitions or ΔpH-dependent quenching of photosystem II fluorescence in red algae. *Biochemistry* **35,** 9435–9445
33. Delphin, E., Duval, J. C., Etienne, A. L., and Kirilovsky, D. (1998) ΔpH-dependent photosystem II fluorescence quenching induced by saturating, multiturnover pulses in red algae. *Plant Physiol.* **118,** 103–113
34. Vass, I., and Cser, K. (2009) Janus-faced charge recombinations in photosystem II photoinhibition. *Trends Plant Sci.* **14,** 200–205
35. Krieger, A., Moya, I., and Weis, E. (1992) Energy-dependent quenching of chlorophyll-a fluorescence. Effect of pH on stationary fluorescence and picosecond-relaxation kinetics in thylakoid membranes and photosystem-II preparations. *Biochim. Biophys. Acta* **1102,** 167–176
36. Bruce, D., Samson, G., and Carpenter, C. (1997) The origins of nonphotochemical quenching of chlorophyll fluorescence in photosynthesis. Direct quenching by P680(+) in photosystem II enriched membranes at low pH. *Biochemistry* **36,** 749–755
37. Minoda, A., Sakagami, R., Yagisawa, F., Kuroiwa T., and Tanaka, K. (2004) Improvement of culture conditions and evidence for nuclear transformation by homologous recombination in a red alga, *Cyanidioschyzon merolae* 10D. *Plant Cell Physiol.* **45,** 667–671
38. Adachi, H., Umena, Y., Enami, I., Henmi, T., Kamiya, N., and Shen, J. R. (2009) Towards structural elucidation of eukaryotic photosystem II. Purification, crystallization and preliminary x-ray diffraction analysis of photosystem II from a red alga. *Biochim. Biophys. Acta* **1787,** 121–128
39. Cunningham, F. X., Jr., Lee, H., and Gantt, E. (2007) Carotenoid biosynthesis in the primitive red alga *Cyanidioschyzon merolae*. *Eukaryot. Cell* **6,** 533–545
40. Oren, A., Kühl, M., and Karsten, U. (1995) An endoevaporitic microbial mat within a gypsum crust. Zonation of phototrophs, photopigments, and light penetration. *Mar. Ecol. Prog. Ser.* **128,** 151–159
41. Rudowska, Ł., Gieczewska, K., Mazur, R., Garstka, M., and Mostowska, A. (2012) Chloroplast biogenesis. Correlation between structure and function. *Biochim. Biophys. Acta.* **1817,** 1380–1387
42. Kaminskaya, O., Kern, J., Shuvalov, V. A., and Renger, G. (2005) Extinction coefficients of cytochromes b_{559} and c_{550} of *Thermosynechococcus elongatus* and cyt b_{559}/PS II stoichiometry of higher plants. *Biochim. Biophys. Acta* **1708,** 333–341
43. Quigg, A., Kotabová, E., Jarešová, J., Kaňa, R., Setlík, J., Sedivá, B., Komárek, O., and Prášil, O. (2012) Photosynthesis in *Chromera velia* represents a simple system with high efficiency. *PLoS One* **7,** e47036
44. Kolber, Z. S., Prasil, O., and Falkowski, P. G. (1998) Measurements of variable chlorophyll fluorescence using fast repetition rate techniques. Defining methodology and experimental protocols. *Biochim. Biophys. Acta* **1367,** 88–106
45. Schägger, H., and von Jagow, G. (1987) Tricine-sodium dodecyl sulfate-polyacrylamide gel electrophoresis for the separation of proteins in the range from 1 to 100 kDa. *Anal. Biochem.* **166,** 368–379
46. Schägger, H. (2006) Tricine-SDS-PAGE. *Nat. Protoc.* **1,** 16–22
47. Oostergetel, G. T., Keegstra, W., and Brisson, A. (1998) Automation of specimen selection and data acquisition for protein electron crystallography. *Ultramicroscopy* **74,** 47–59
48. van Heel, M. (1987) Similarity measures between images. *Ultramicroscopy* **21,** 95–100
49. Bumba, L., Havelková-Dousová, H., Husák, M., and Vácha, F., (2004) Structural characterization of photosystem II complex from red alga *Porphyridium cruentum* retaining extrinsic subunits of the oxygen-evolving complex. *Eur. J. Biochem.* **271,** 2967–2975
50. Dixon, M. (1953) The determination of enzyme inhibitor constants. *Biochem. J.* **55,** 170–171
51. Lavergne, J. (1982) Mode of action of 3-(3,4-dichlorophenyl)-1,1-dimethylurea. Evidence that the inhibitor competes with plastoquinone for binding to a common site on the acceptor side of photosystem II. *Biochim. Biophys. Acta* **682,** 345–353
52. Boussac, A., Sugiura, M., and Rappaport, F. (2011) Probing the quinone binding site of photosystem II from *Thermosynechococcus elongatus* containing either PsbA1 or PsbA3 as the D1 protein through the binding characteristics of herbicides. *Biochim. Biophys. Acta* **1807,** 119–129
53. Koua, F. H., Umena, Y., Kawakami, K., and Shen, J. R. (2013) Structure of Sr-substituted photosystem II at 2.1 A resolution and its implications in the mechanism of water oxidation. *Proc. Natl. Acad. Sci. U.S.A.* **110,** 3889–3894
54. Kaňa, R., Kotabová, E., Komárek, O., Šedivá, B., Papageorgiou, G. C., Govindjee, and Prášil, O. (2012) The slow S to M fluorescence rise in cyanobacteria is due to a state 2 to state 1 transition. *Biochim. Biophys. Acta* **1817,** 1237–1247
55. Shen, J. R., and Kamyía, N. (2000) Crystallization and the crystal properties of the oxygen-evolving photosystem II from *Synechococcus vulcanus*. *Biochemistry* **39,** 14739–14744

56. Boussac, A., Rappaport, F., Carrier, P., Verbavatz, J. M., Gobin, R., Kirilovsky, D., Rutherford, A. W., and Sugiura, M. (2004) Biosynthetic Ca^{2+}/Sr^{2+} exchange in the photosystem II oxygen-evolving enzyme of *Thermosynechococcus elongatus*. *J. Biol. Chem.* **279,** 22809–22819
57. Roose, J. L., Kashino, Y., and Pakrasi, H. B. (2007) The PsbQ protein defines cyanobacterial photosystem II complexes with highest activity and stability. *Proc. Natl. Acad. Sci. U.S.A.* **104,** 2548–2553
58. Cullen, M., Ray, N., Husain, S., Nugent, J., Nield, J., and Purton, S. (2007) A highly active histidine-tagged *Chlamydomonas reinhardtii* photosystem II preparation for structural and biophysical analysis. *Photochem. Photobiol. Sci.* **6,** 1177–1183
59. Wang, Z. G., Xu, T. H., Liu, C., and Yang, C. H. (2010) Fast isolation of highly active photosystem II core complexes from spinach. *J. Integr. Plant Biol.* **52,** 793–800
60. Pagliano, C., Chimirri, F., Saracco, G., Marsano, F., and Barber, J. (2011) One-step isolation and biochemical characterization of a highly active plant PSII monomeric core. *Photosynth. Res.* **108,** 33–46
61. de Groot, H. J. (2010) Integration of catalysis with storage for the design of multi-electron photochemistry devices for solar fuel. *Appl. Magn. Reson.* **37,** 497–503
62. Nocera, D. G. (2012) The artificial leaf. *Acc. Chem. Res.* **45,** 767–776
63. Telfer, A. (2005) Too much light? How β-carotene protects the photosystem II reaction centre. *Photochem. Photobiol. Sci.* **4,** 950–956
64. Kok, B. (1956) On the inhibition of photosynthesis by intense light. *Biochim. Biophys. Acta* **21,** 234–244
65. Aro, E. M., Virgin, I., and Andersson, B. (1993) Photoinhibition of photosystem II. Inactivation, protein damage and turnover. *Biochim. Biophys. Acta* **1143,** 113–134
66. Long, S. P., Humphries, S., and Falkowski, P. G. (1994) Photoinhibition of photosynthesis in nature. *Annu. Rev. Plant Physiol. Plant Mol. Biol.* **45,** 633–662
67. Frank, H. A., and Cogdell, R. J. (1993) Photochemistry of carotenoids. in *Carotenoids in Photosynthesis* (Young, A., and Britton, G., eds) pp. 252–326, Chapman and Hall, London
68. Szabó, I., Bergantino, E., and Giacometti, G. M. (2005) Light and oxygenic photosynthesis. Energy dissipation as a protection mechanism against photo-oxidation. *EMBO Rep.* **6,** 629–634
69. Santabarbara, S., Casazza, A. P., Ali, K., Economou, C. K., Wannathong, T., Zito, F., Redding, K. E, Rappaport, F., and Purton, S. (2013) The requirement for carotenoids in the assembly and function of the photosynthetic complexes in *Chlamydomonas reinhardtii*. *Plant Physiol.* **161,** 535–546
70. Sozer, O., Komenda, J., Ughy, B., Domonkos, I., Laczkó-Dobos, H., Malec, P., Gombos, Z., and Kis, M. (2010) Involvement of carotenoids in the synthesis and assembly of protein subunits of photosynthetic reaction centers of *Synechocystis* sp. PCC 6803. *Plant Cell Physiol.* **51,** 823–835
71. Dall'Osto, L., Holt, N. E., Kaligotla, S., Fuciman, M., Cazzaniga, S., Carbonera, D., Frank, H. A., Alric, J., and Bassi, R. (2012) Zeaxanthin protects plant photosynthesis by modulating chlorophyll triplet yield in specific light-harvesting antenna subunits. *J. Biol. Chem.* **287,** 41820–41834
72. Koblizek, M., Ciscato, M., Komenda, J., Kopecky, J., Siffel, P., and Masojidek, J. (1999) Photoadaptation in the green alga *Spongiochloris* sp. A three-fluorometer study. *Photosynthetica* **37,** 307–323
73. Holt, N. E., Zigmantas, D., Valkunas, L., Li, X. P., Niyogi, K. K., and Fleming, G. R. (2005) Carotenoid cation formation and the regulation of photosynthetic light harvesting. *Science* **307,** 433–436
74. Johnson, M. P., Havaux, M., Triantaphylidès, C., Ksas, B., Pascal, A. A., Robert, B., Davison, P. A., Ruban, A. V., and Horton, P. (2007) Elevated zeaxanthin bound to oligomeric LHCII enhances the resistance of *Arabidopsis* to photooxidative stress by a lipid-protective, antioxidant mechanism. *J. Biol. Chem.* **282,** 22605–22618
75. Havaux, M., Dall'osto, L., and Bassi, R. (2007) Zeaxanthin has enhanced antioxidant capacity with respect to all other xantophylls in *Arabidopsis* leaves and functions independent of binding to PSII antennae. *Plant Physiol.* **145,** 1506–1520
76. Havaux, M. (1998) Carotenoids as membrane stabilizers in chloroplasts. *Trends Plant Sci.* **3,** 147–151
77. Gruszecki, W. I., and Strzałka, K. (2005) Carotenoids as modulators of lipid membrane physical properties. *Biochim. Biophys. Acta* **1740,** 108–115
78. Cunningham, F. X., Dennenberg, R. J., Mustardy, L., Jursinic, P. A., and Gantt, E. (1989) Stoichiometry of photosystem I, photosystem II, and phycobilisomes in the red alga *Porphyridium cruentum* as a function of growth irradiance. *Plant Physiol.* **91,** 1179–1187
79. Cunningham, F. X., Jr., and Gantt, E. (2005) A study in scarlet. Enzymes of ketocarotenoid biosynthesis in the flowers of *Adonis aestivalis*. *Plant J.* **41,** 478–492
80. Cser, K., and Vass, I. (2007) Radiative and non-radiative charge recombination pathways in photosystem II studied by thermoluminescence and chlorophyll fluorescence in the cyanobacterium *Synechocystis* 6803. *Biochim. Biophys. Acta* **1767,** 233–243
81. Kargul, J., Boehm, M., Morgner, N., Robinson, C. V., Nixon, P. J., and Barber, J. (2012) Compositional and structural analyses of the photosystem II from the red alga *Cyanidioschyzon merolae.* in *Photosynthesis: Research for Food, Fuel and Future* (Lu, C., Zhang, L., and Kuang, T., eds) pp. 59–63, Zhejiang University Press/Springer-Verlag, Hangzhao, Beijing, China
82. Kuhl, H., Rögner, M., Van Breemen, J. F., and Boekema, E. J. (1999) Localization of cyanobacterial PS II donor-side subunits by electron microscopy and the supramolecular organization of PS II in the thylakoid membrane. *Eur. J. Biochem.* **266,** 453–459
83. Arteni, A. A., Nowaczyk, M., Lax, J., Kouril, R., Rögner, M., and Boekema, E. J. (2005) Single particle electron microscopy in combination with mass spectrometry to investigate novel complexes of membrane proteins. *J. Struct. Biol.* **149,** 325–331
84. Nowaczyk, M. M., Hebeler, R., Schlodder, E., Meyer, H. E., Warscheid, B., and Rögner, M. (2006) Psb27, a cyanobacterial lipoprotein, is involved in the repair cycle of photosystem II. *Plant Cell* **18,** 3121–3131
85. Shi, L. X., Lorković, Z. J., Oelmuller, R., and Schroder, W. P. (2000) The low molecular mass PsbW protein is involved in the stabilization of the dimeric photosystem II complex in *Arabidopsis thaliana*. *J. Biol. Chem.* **275,** 37945–37950